The effect of liquid nitriding on the corrosion resistance of AISI 304 austenitic stainless steel in H2S environments

Li, Longyi; Wang, Jun ; Yan, Jing; Duan, Liang; Li, Xiaoying; Dong, Hanshan

[Link to publication on Research at Birmingham portal](#)

The effect of liquid nitriding on the corrosion resistance of AISI 304 austenitic stainless steel in H₂S environments

Longyi Li [a], Jun Wang [a*], Jing Yan [b], Lian Duan [a], Xiaoying Li [c], Hanshan Dong [c]

a College of Manufacturing Science and Engineering, Sichuan University, 610065, Chengdu, PR China

b Research Institute of Natural Gas Technology, PetroChina Southwest Oil and Gas Field Company, 610213, Chengdu, PR China.

c School of Metallurgy and Materials, University of Birmingham, Edgbaston, Birmingham B15 2TT, UK

Abstract: AISI 304 austenitic stainless steel was low-temperature liquid nitrided in a molten salt bath at 703 K for 8 h, which produced a 3-layered structure consisting of a top oxide layer, an intermediate nitrogen-rich layer and a bottom carbon-rich layer. The effect of nitriding on its corrosion resistance was investigated in a H₂S environment. The corrosion rate of the untreated sample is about 3.3 times that of the nitrided sample after H₂S corrosion. Corrosion pits can be clearly observed on the surface of the untreated sample, while the nitrided sample surface remained relatively intact. Both the oxide layer and the nitrogen-rich layer can help reduce the hydrogen permeation, which is beneficial for combating hydrogen embrittlement. The corrosion products mainly consisted of oxides, hydroxides, and sulfates. The nitrided layers can serve as a barrier to corrosion, thus preventing the corrosion of the substrate material. Active nitrogen in the nitrided layer reacts with H ions to form NH₄⁺, which effectively prevents further acidification of the local area and inhibits the occurrence of pitting corrosion and the dissolution rate of the metal in the etching hole, thus improving the local corrosion resistance of the stainless steel.

Key words: austenite stainless steels, expand austenite, corrosion resistance, liquid nitriding, surface treatment

1. Introduction

Austenite stainless steel is widely used in various industrial fields due to its excellent corrosion resistance and mechanical properties. With the increasing exploitation and processing of high sulfur oil and gas field, H₂S corrosion has become a widespread concern.[1] H₂S is one of the most dangerous factors causing metal corrosion in acidic oil and gas environments, and electrochemical corrosion will occur on the surface of the pipeline used.[2] In recent years, many researchers have conducted extensive research on the local corrosion and stress corrosion cracking (SCC) mechanism of stainless steel in H₂S medium. The research was focused on the

40 structure, properties, formation process and external factors of corrosion products in
41 saturated H_2S systems.[3-6] Ding et al. investigated the behavior of corrosion and SCC
42 of austenitic stainless steels in high $H_2S–CO_2–Cl^-$ environments. [7] Their results
43 showed that high $H_2S–CO_2$ pressure can accelerate anodic dissolution process,
44 deteriorate passive films, and aggravate SCC sensitivity. The corrosion rate of steel in
45 wet H_2S is significantly higher than that in dry H_2S environment.[8] H_2S reacted with
46 metals to form surface metal sulfides, and released hydrogen atoms, which were
47 absorbed by the metal surface and caused hydrogen embrittlement.[9] Besides, low pH
48 can promote both cathodic and anodic actions on stainless steel and facilitate passive
49 film breakdown. [7]

50   In addition to the corrosion of H_2S, CO_2 and Cl^-, saturated natural gas in
51 pipelines will have a free liquid phase due to the effect of pressure drop, and a certain
52 amount of solid impurities will be mixed in the pipeline, resulting in three-phase
53 coexistence of gas, solid, and liquid. Erosion-corrosion is faster than corrosion alone
54 and is a more hazardous local corrosion.[10] When corrosive liquid contains solid
55 particles (such as insoluble salts, sand, drilling fluid, etc.), it is more likely to cause
56 such erosion-corrosion damage. Austenitic stainless steels have a low carbon content
57 (mass fraction below 0.03 %), resulting in a low surface hardness and poor wear
58 resistance. The service life of stainless steel pipes under such conditions will be
59 seriously reduced，and so it is necessary to improve their surface hardness and
60 strength on the premise of ensuring its good comprehensive performance.

61   It has been reported previously that austenitic stainless steels are
62 thermochemically treated (carburized or nitrided) at low temperatures to form
63 interstitial atoms supersaturated non-deposition layers. [11-12] After the treatment, a
64 layer with a high concentration of nitrogen and/or carbon will be formed on the
65 surface of the treated austenitic stainless steel. This surface layer can effectively
66 improve the hardness, wear resistance, fatigue resistance and corrosion resistance of
67 the material, which is so-called S-phase or expanded austenite.[12] Low-temperature
68 nitriding has been shown to significantly improve pitting potential. Dong discovered
69 that low temperature nitrided 316 stainless steel showed excellent resistance to pitting
70 of chlorine containing solution, and the increased corrosion resistance of the nitride S
71 phase layer is thought to be due to its high nitrogen content.[13] The enhancement in
72 corrosion resistance of austenitic stainless steels by nitriding or carbonization
73 treatment may be related to a high surface interstitial atom concentration or a large
74 surface residual compressive stress due to interstitial atoms.[14]

75   Zhang et al. performed Quench-Polish-Quench (QPQ) salt bath compound
76 treatment on GX-8 alloy steel and found that the dense oxide film Fe_3O_4 could
77 significantly reduce the friction coefficient of the material at 573 K, and the corrosion
78 resistance of the material was greatly improved before the oxide film was ruptured.[15]
79 However, the QPQ treatment is a multi-step and hence relatively complicated process.
80 In contrast, low-temperature salt bath nitriding does not require an additional
81 oxidation process to form a surface oxide layer. Hence, the salt bath nitriding process
82 is simpler and the cost of the equipment is lower than the QPQ process.
83   The aim of the present paper was to study the effect of low-temperature liquid

bath nitriding on the corrosion resistance of AISI 304 austenitic stainless steel in a H_2S containing environment. Through the H_2S immersion corrosion tests, the corrosion behavior and the corrosion mechanism of low temperature salt bath nitride 304 austenitic stainless steel in H_2S containing environments (such as pipelines for oil and gas applications) were studied. The low-temperature nitriding is expected to be applied to the pipelines used for oil-gas fields, significantly extending their service life in the H_2S corrosion environment.

2. Experimental

2.1 Material

The material used in this experiment was cast 304 stainless steel, taken from the natural gas valve castings supplied by Southwest Natural Gas Research Institute , China. The chemical composition provided by the materials supplier is shown in Table 1. The samples were ground with abrasive papers from 400# down to 1200#, degreased with a mixture of 50 vol% ethanol and 50 vol% acetone, and finally washed with deionized water and dried in atmosphere.

Table 1 Chemical composition of AISI 304 stainless steel (mass%)

Element	C	Cr	Ni	Mn	Si	S	P	Fe
Pct	0.035	18.640	8.010	1.100	0.436	0.020	0.013	Balance

2.2 Liquid bath nitriding and H_2S corrosion test

The chemicals used in this experiment for liquid bath nitriding were non-toxic cyanate, chloride and carbonate salts. The nitriding process involved immersing the sample in 703 K molten salt for 8 hours, during which the non-toxic cyanate decomposes into carbon atoms and nitrogen atoms, forming a high chemical potential on the surface of the samples. More details can be found in literature.[16] This high chemical potential promotes the diffusion of the nitrogen and carbon atoms into the austenitic stainless steel sample, thus forming a large supersaturation of N(C) in its surface.

H_2S corrosion tests were conducted in accordance with NACE TM0177-2005 standard using the solution 'A' recommended by NACE TM0177-2005. Both the untreated and nitrided samples were soaked in this solution for 720 hours.

Before the H_2S corrosion test, the mass of the sample (m) was weighed and recorded. At the end of the test, the corroded sample was taken out, and the corrosion product formed on the surface was removed with an acid stripping solution (500 ml HCl + 500 ml H_2O + 3.5 g $C_6H_{12}N_4$). The sample was degreased with acetone and then dried in a box. After drying for 24 hours, the sample was taken out for weighing (m_t), and the corrosion rate was calculated based on the weight loss during the test. The uniform corrosion rate (R_{corr}) is calculated as follows: $R_{corr}=8.76\times10^4\times(m-m_t)/(S_1\times\rho\times t)$, where S_1 is the total area of the test piece (32 cm^2); ρ is the density of the test piece material (7.9 g/cm^3); and t is the test time (720 h).

2.3 Hydrogen permeation test

Hydrogen permeation testing was performed in line with ASTM G148 standard using a type Avanathan-Stachursky double-electrolytic cell produced by Wuhan Corrtest, China.[17] Three sets of samples were prepared: untreated samples, as-nitrided samples and the nitride samples whose surface oxide film was removed by mechanical polishing. The samples used in this test were stainless steel wafer electrodes with a working surface of 1.77 cm^2 and a thickness of 0.2 mm. The experimental conditions were decided by referring to literature.[18-19] The experimental solution is 0.5 mol/L sulfuric acid with 1 g/L CH_4N_2S, and the hydrogen charge current is 20 mA/cm^2 with an anode potential of 300 mV. Before the test solution was added, the sample was passivated in a 0.2 mol/L NaOH solution for more than 24 h, in order that the background current density is less than 0.1 $\mu A/cm^2$.[20]

The hydrogen diffusion flux ($J\infty$) is calculated from the anode steady-state current (I_∞) and can be expressed as:

$$J\infty = \quad [21]$$

Where: A is the area of the sample in contact with the solution; F is the Faraday constant.

The effective hydrogen diffusion coefficient (D_{eff}) can be calculated using the formula below:

$$D_{eff} = \quad [22]$$

Where: t is the thickness of the sample; t_L is the delay time. The delay time is approximately equal to the time taken for the hydrogen charging current density to reach 0.63 times the steady-state anode current density, i.e. the time used for $I_a = 0.63I\infty$. The hydrogen concentration C_o at the hydrogen end can be estimated by the following formula:

$$C_o = \quad [22]$$

2.4 Microstructural characterization

The cross section of the sample before and after the H_2S corrosion tests was mechanically polished and chemically etched with an etchant formulated with 50 vol% HCl, 25 vol% HNO_3, and 25 vol% H_2O. The OLYMPUS GX51 optical microscope and JSM-7500F scanning electron microscope were used for microstructural analysis. The surface phases were studied using the EMPYREAN X-ray diffractometer (XRD) with a scanning range of 20 to 110 degrees with Cu Kα radiation ($\lambda = 0.15418nm$). The SHIMADZU-1720 electron probe microanalyzer (EPMA) was used to quantitatively analyze the elemental distribution from the surface to the matrix. X-ray photoelectron spectroscopy (XPS) was used to analyze the surface corrosion products.

3. Results

3.1 Characteristics of the nitrided layers

1. Top oxide layer

2. Nitride + S-phase

3. Carbon-rich S-phase sublayer

Substrate
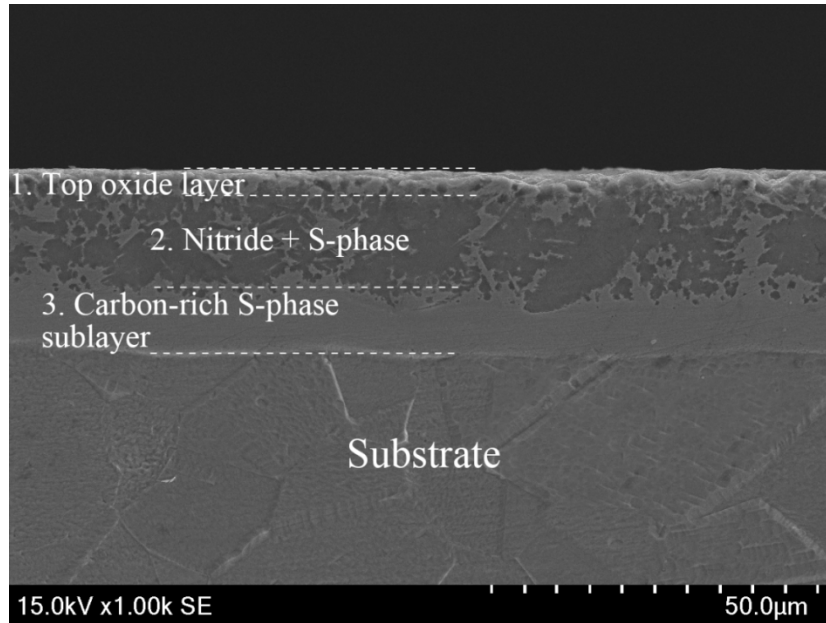
15.0kV x1.00k SE   50.0μm

Fig.1 A typical cross sectional SEM image of nitrided sample

Figure 1 shows the cross-sectional photomicrograph of the AISI304 austenitic stainless steel after low-temperature salt bath nitriding treatment. The substrate shows clear grain boundaries after etching with the etchant. The salt bath nitriding produced a 3-layered structure consisting of an oxide top layer, followed by a nitrogen-rich layer and a carbon-rich layer. The atomic nitrogen was formed from the following CNO^- dissociation reaction: $4CNO^- \rightarrow 2CN^- + CO_3^{2-} + CO + [N]$. Carburizing is also promoted by the liberation of atomic carbon species according to the following CO dissociation reaction: $CO \rightarrow CO_2 + [C]$. Under the same treatment conditions, the thickness of the nitrided layer is larger than that of the carburized layer. This is mainly due to the fact that the atomic radius of N is smaller than that of the C atom, and the energy required for N atoms to enter the lattice is smaller than that for C atoms. Under the same conditions, the nitrogen atoms can diffuse deeper that carbon atoms. Tsujikawa et al. used simultaneous carburizing and nitriding process to obtain a similar layer on the surface of austenitic stainless steel.[23] Due to the long processing time, certain Cr nitrides appear in the nitrided layer.

3.2 Corrosion morphology and corrosion rate

Nitrided samples and as-received 304 samples were immersed in H_2S solution for 720 h and the cross-sectional micrographs are shown in the Figure 2.

As shown in Figure 2(a), a number of pits and cracks were observed from the cross-section of the untreated sample, which indicates pitting and cracking of the sample. In the process of crack propagation, the width and depth of the crack continuously increased, and the outer layer material eventually spalled off. In contrast, neither pits nor cracks were observed from the cross-section of the nitrided samples after H_2S corrosion test (Fig.2(b)).
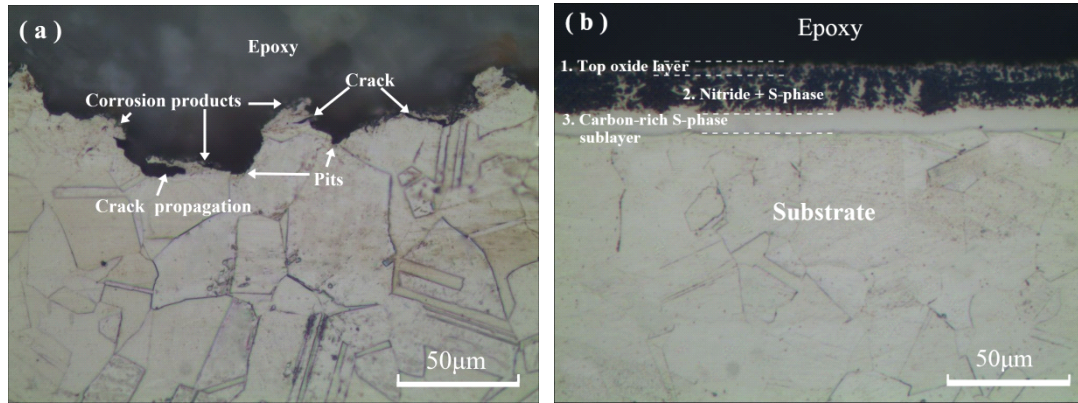
5

189

190 **Fig.2** Cross-sectional optical micrographs (OM): (a) untreated sample (b) nitrided sample after

191 immersion in H_2S solution for 720h

192   Figure 3 shows the surface morphology of the untreated and nitrided samples after

193 immersion in H_2S solution for 720h. Many agglomerates were formed on the surface

194 of the untreated sample (Fig.3(a)), which is generally considered to be corrosion

195 product FeS. The surface of the nitrided sample remained intact as evidenced by the

196 existence of the original grinding marks with almost no corrosion product (Fig.3(b)).
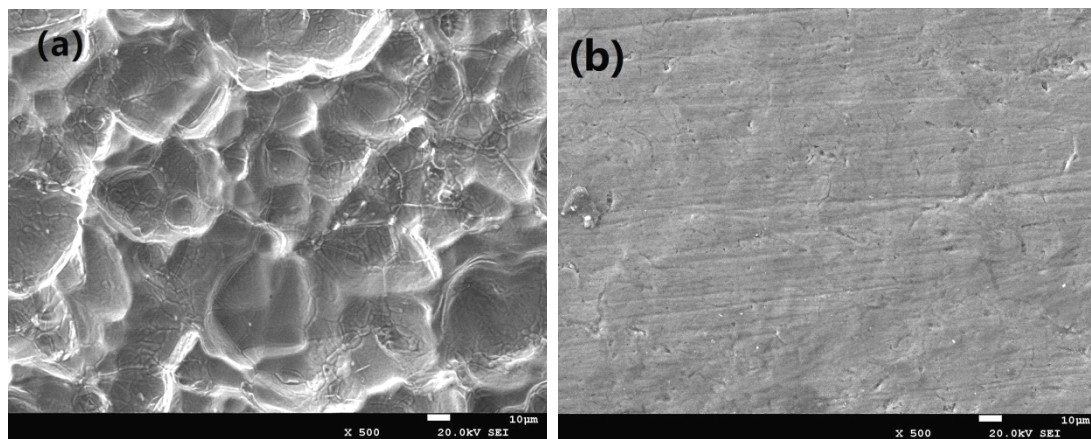

197

198 **Fig.3** SEM surface corrosion morphology: (a) untreated sample (b) nitrided sample after

199 immersion in H_2S solution for 720h

200   As shown in Figure 4, the corrosion rate of the untreated 304 austenitic stainless

201 steel (0.20 mm/a) is approximately 3.3 times that of the nitrided samples (0.06 mm/a).

202 This indicates that the nitriding treatment can significantly improve the corrosion

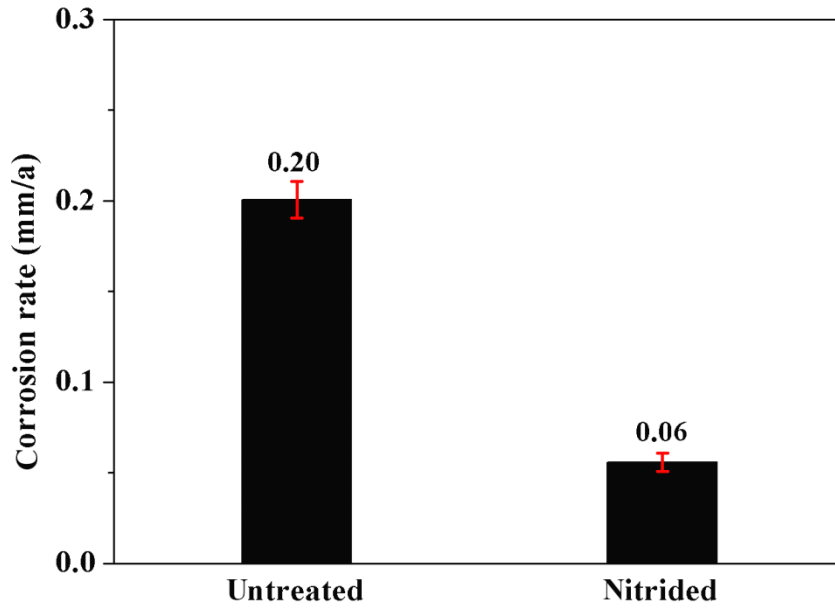203 resistance of 304 stainless steel in the H_2S environment.

204

205

206

207

208

209

210   The ionization of H$_2$S in the solution produced a large amount of H$^+$, which led to
211 a significant decrease in the pH of the solution. The ionization reaction can be
212 described as follows: H$_2$S $=$ H$^+$ + HS$^-$; 2HS$^-$ $=$ 2H$^+$ + S^{2-}. The ionized H$^+$ is a strong
213 depolarizer that can easily take away electrons from the metal and promote the
214 dissolution reaction of the anode steel to cause metal corrosion. The process of
215 electrochemically etching the cathode and the anode by H$_2$S is as follows:

216   Cathode: Fe - 2 e$^-$ $\rightarrow$ Fe^{2+};
217   Anode: 2H$^+$ + 2e$^-$ $\rightarrow$ 2H $\rightarrow$ H$_2$ $\uparrow$.

218   The anode corrosion product is: Fe^{2+} + S^{2-} $=$ FeS$\downarrow$. Therefore, after the steel is
219 corroded by H$_2$S, the final product of the anode is FeS. The product usually has a
220 defective structure with poor adhesion to the surface of steel. Hence, it can be easily
221 detached and oxidized, and has a more positive potential. The corrosion product then
222 acts as a cathode and the matrix to form an active microbattery and continues the
223 corrosion of the steel. The process repeated itself and the layer eventually cracked.
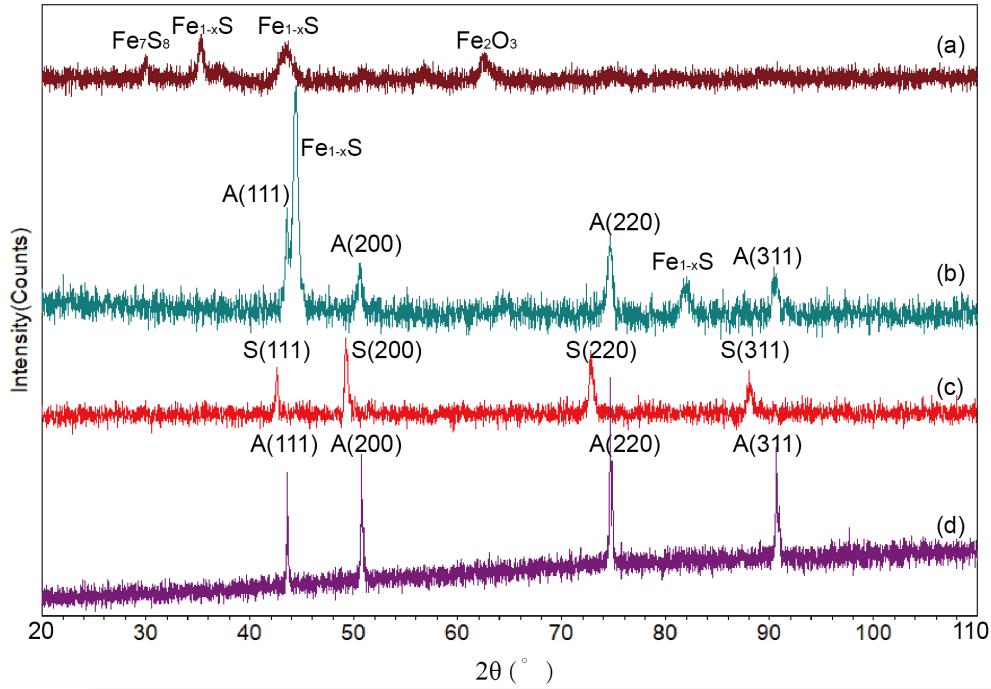
224

225 ## 3.3 XRD analysis

Fig.5 XRD patterns for different samples: (a) nitrided sample after corrosion test, (b) untreated sample after corrosion test, (c) as-nitrided sample and (d) untreated sample before corrosion test
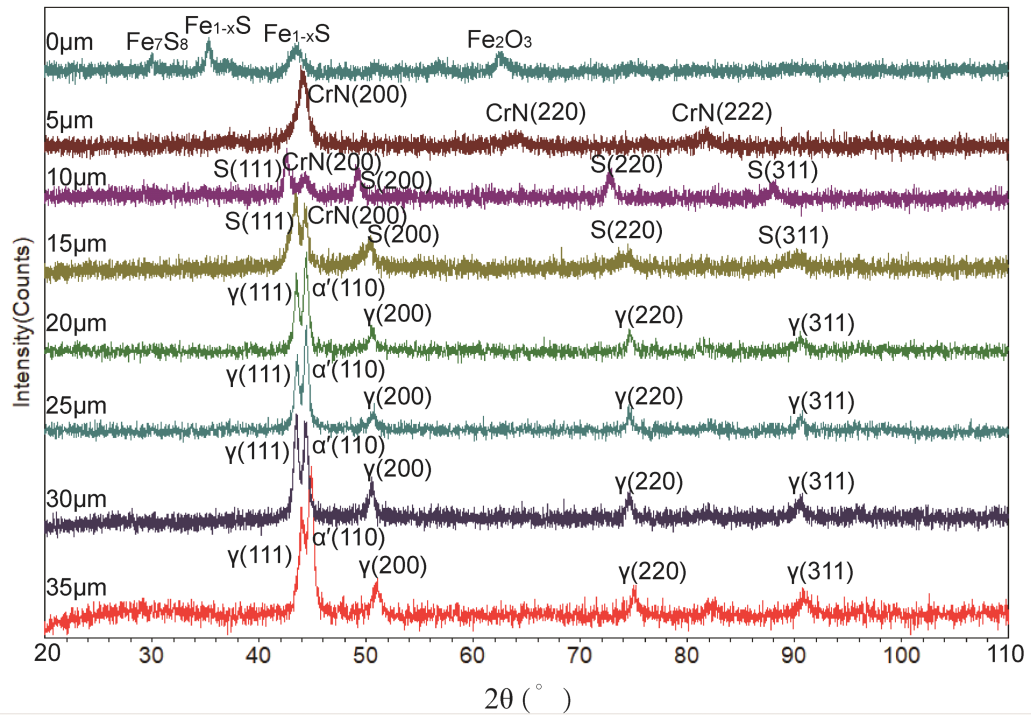

Fig. 6 XRD patterns as a function of the depth below the original nitrided surface (after mechanical material removal).

8

Untreated and nitrided samples were characterized by XRD to identify the phases produced as a consequence of H_2S corrosion process; the diffraction patterns of the samples are shown in Figure 5. It can be seen from Figure 5 that the untreated sample shows typical peaks for austenite (Fig.5(d)); the nitrided sample clearly shows S1(111)、S2(200)、S3(220) and S4(311) peaks. This indicates that the S-phase layer has been successfully produced during nitriding. The N or C atoms dissolved in austenite caused the expansion of the original face-centered cubic lattice of austenite (i.e. expanded austenite) and the left-shift of these peaks.[24] As shown in Figure 5(b), the corrosion product formed on the untreated sample is $Fe_{1-X}S$, which shows two peaks, one near $\gamma(111)$ and the other between $\gamma(200)$ and $\gamma(311)$. Clear austenite characteristic peaks can still be observed on the XRD diffraction pattern of the untreated sample after H_2S corrosion. The corrosion products of the nitrided samples were mainly Fe_7S_8, $Fe_{1-X}S$, and Fe_2O_3. Compared with the untreated samples, the characteristic peaks of the expanded austenite could not be observed. This implies that the nitrogen concentrations in the ≈ 5 μm thick layer below the specimen surface that is sampled by the X-rays would be reduced during the H_2S corrosion test.

The XRD patterns obtained at different depths below the original surfaces are shown in Figure 6. In the depth of 5 μm, the nitrided sample exhibits three main diffraction peaks of CrN, which was formed as a consequence of the temperature of the treatment, the chromium-rich alloy AISI 304, and the high nitrogen content. When the nitrogen content gradually decreased with the depth, the intensity and the number of CrN peaks reduced accordingly. Normally, when the AISI 304 stainless steel is nitride at 703 K or below, the nitrided layer should be free of nitrides. However, the as-cast 304 stainless steel used in this research may not be well annealed after cold rolling, and a large amount of deformed martensite (α') was left in the matrix, as evidenced by the clear α' peak detected from the substrate (Fig. 6).   This resulted in rapid nitrogen diffusion and precipitation of CrN. At the depth of 10 and 15 μm, distinct peaks of S phase and a weak CrN peak can be detected. Then, the α'-martensite phase was detected from the depth 20 μm down to the substrate, which is also contributed by the strain-induced martensite formed during the layer-by-layer mechanical polishing process. Starting from the depth of 20μm, as the interstitial atom concentration gradually decreased, the lattice distortion also gradually decreased, and it is better to call it γ-phase instead of S-phase. The content of interstitial atoms (C or N) continuously decreased with the depth and the diffraction angle of the γ-phase gradually returned to normal values.
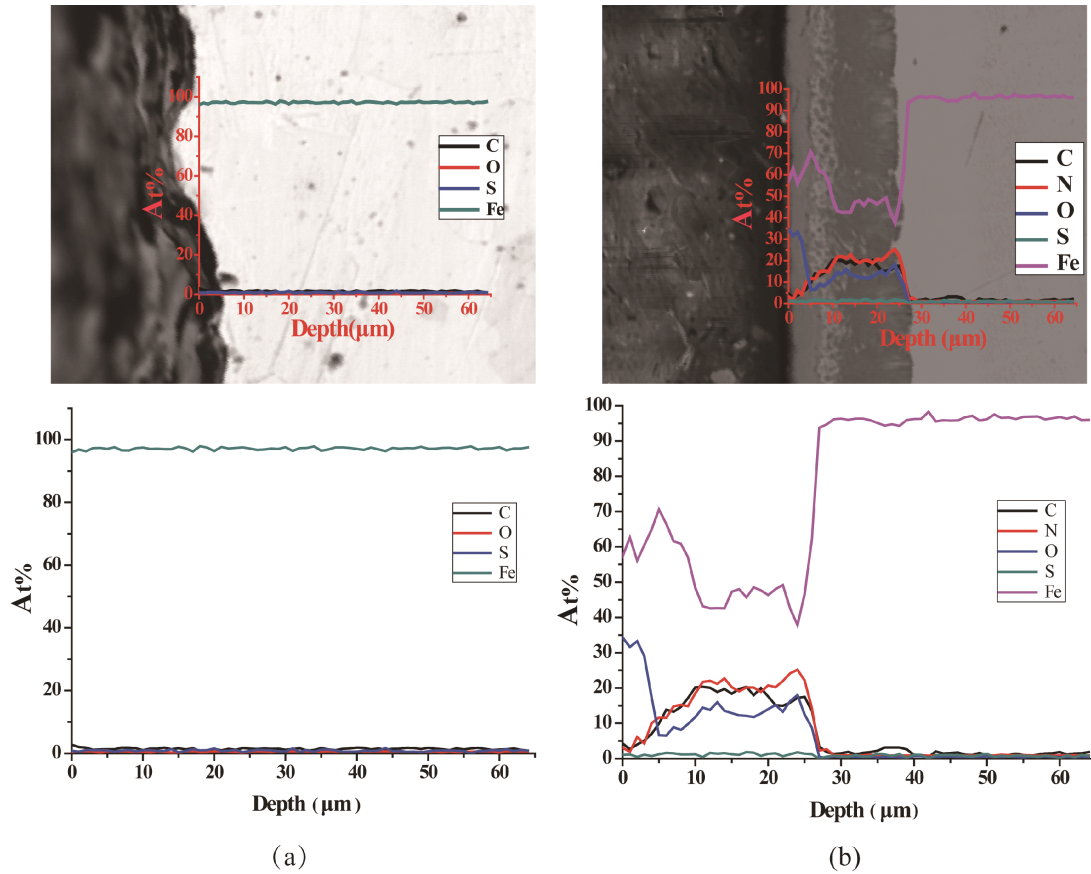
3.4 EPMA analysis

Figure 7 shows the EPMA results of the untreated and low temperature nitrided samples after immersion corrosion test. It can be seen by comparing Figure 7(b) with (a) that oxygen concentration increased significantly in the nitrided layer due to the oxygen atoms introduced during the nitriding process. It can be also seen that there is an oxygen plateau near the surface, which is overlapped with the grey surface layer showed in the top graph of Figure 7(b). This indicates the formation of an oxide layer during the salt bath nitriding process. The concentration of nitrogen was increased due to the formation of supersaturated austenite, which improves corrosion resistance. However, the nitrogen content decreased slightly near the surface, which may be caused by the consumption of nitrogen atoms. Combined with the results of XPS analysis, it is known that this is due to the reaction of reactive nitrogen in the nitride layer with H^+ in the H_2S solution to form NH_4^+. For the untreated sample, the iron concentration sharply declined on the surface, which means the destruction of the passivation film，thus jeopardizing the corrosion resistance of the untreated sample leading to the appearance of a large number of corrosion pits on the surface (Fig.2(a)).

3.5 XPS analysis

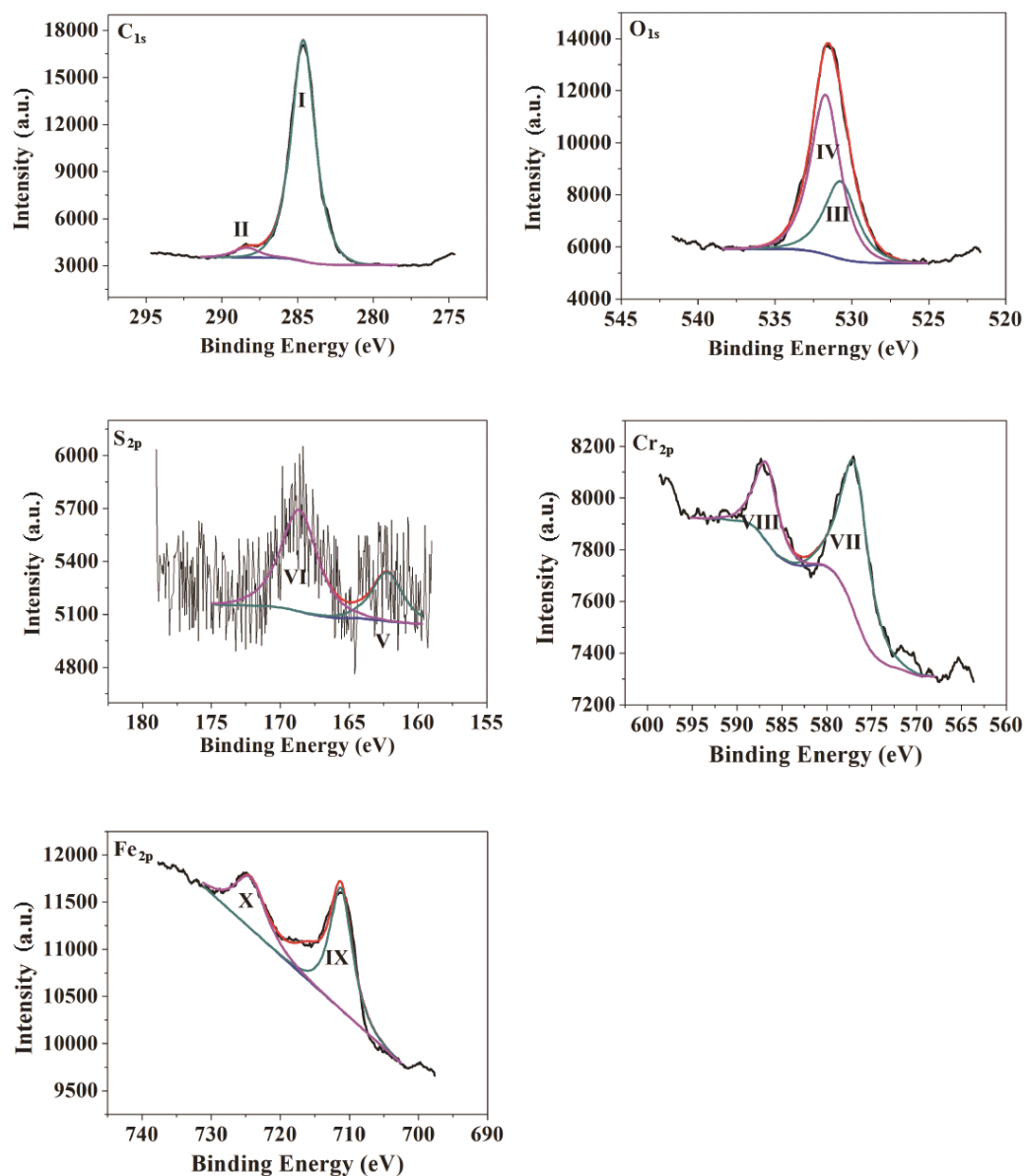**Fig.8** High resolution XPS spectra of untreated samples after H$_2$S corrosion: C$_{1s}$, O$_{1s}$, S$_{2p}$, Cr$_{2p}$, Fe$_{2p}$.
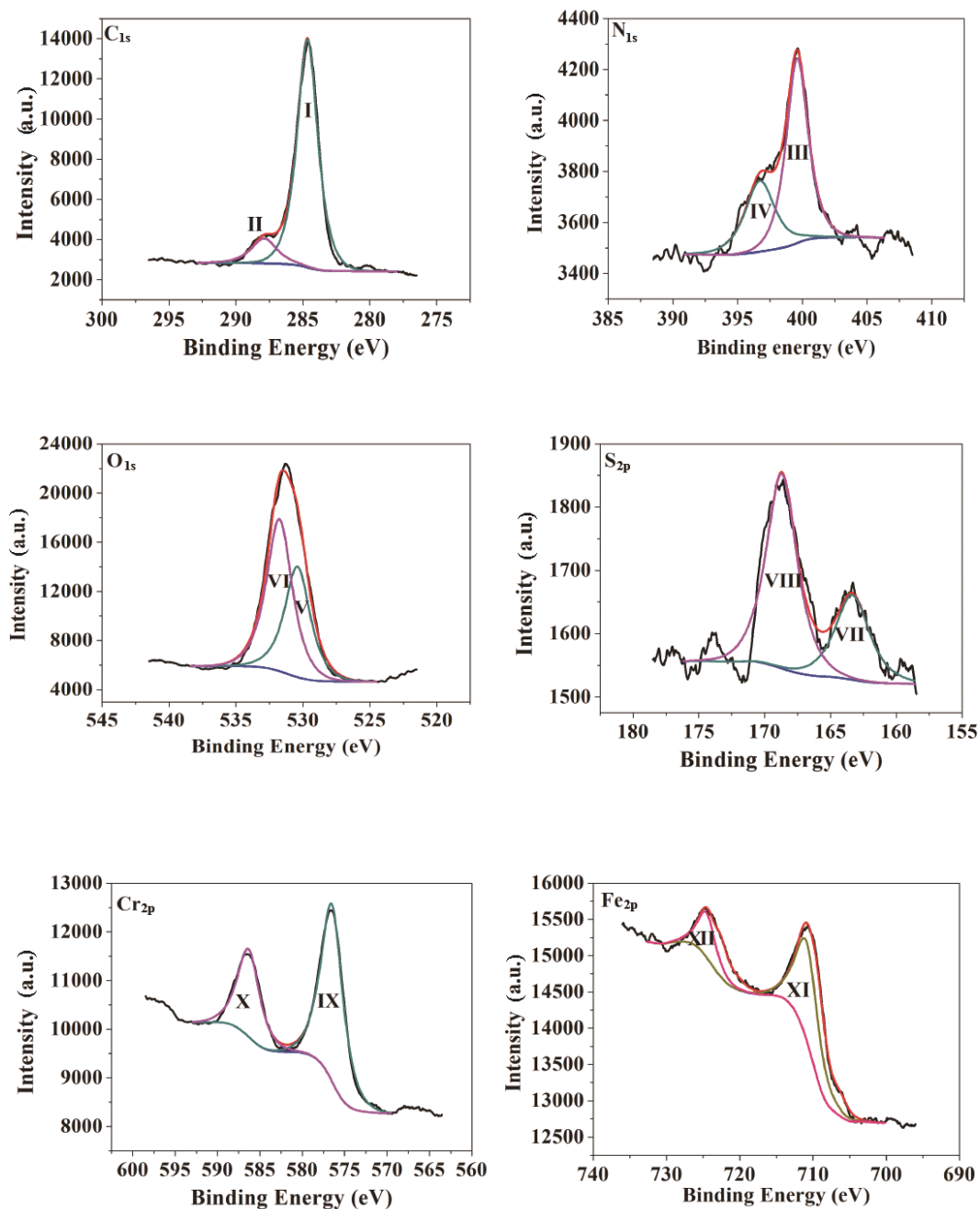
Fig.9 High resolution XPS spectra of nitrided samples after H₂S corrosion: C$_{1s}$, N$_{1s}$, O$_{1s}$, S$_{2p}$, Cr$_{2p}$, Fe$_{2p}$.

Table2 Binding energy and specification for the elements by XPS analysis of nitrided and untreated samples after H₂S corrosion

Element		BE(eV)	peak	at%
untreated				
C	1s	284.6	Adventitious/C , I	19.79
	1s	288.3	Adventitious，II	1.89
O	1s	530.7	Cr_2O_3 , III	15.46
	1s	531.7	FeOOH , IV	28.91
S	2p	162.2	FeS_2 , V	3.78
	$2p_{3/2}$	168.6	SO_4^{2-} , VI	9.40
Cr	$2p_{3/2}$	576.8	Cr_2O_3 , VII	3.90
	$2p_{1/2}$	586.8	$Cr(OH)_3$, VIII	1.66
Fe	$2p_{3/2}$	711.2	Fe_2O_3 , IX	9.65
	$2p_{1/2}$	724.3	FeOOH , X	5.56
nitrided				
C	1s	284.6	Adventitious/C, I	45.04
	1s	288.3	Adventitious，II	6.07
N	1s	396.7	CrN , III	0.98
	1s	399.6	NH_4^+, IV	1.89
O	1s	530.7	Cr_2O_3 , V	16.78
	1s	531.7	FeOOH , VI	23.16
S	$2p_{1/2}$	163.5	FeS_2 , VII	0.10
	$2p_{3/2}$	168.6	SO_4^{2-}, VIII	0.20
Cr	$2p_{3/2}$	576.5	Cr_2O_3 , IX	2.58
	$2p_{1/2}$	586.3	Cr_2O_3 , X	1.27
Fe	$2p_{3/2}$	710.8	Fe_2O_3 , XI	1.42
	$2p_{1/2}$	724.3	FeOOH , XII	0.51

Elemental contributions analyses have been performed for carbon，nitrogen，oxygen, sulfur，chromium and iron on the H_2S corrosion tested surface of untreated and as-nitrided samples and the results are reported in Figure 8 and Figure 9, respectively. The parameters and corresponding atomic contents are detailed in Table 2.

Oxygen (O_{1s}) contribution in both untreated and nitrided sample appears as two visible although entangling peaks: one for oxides at 530.7 eV and one for hydroxides at 531.7 eV.[25] XPS analysis results showed that the corrosion products formed on the untreated and nitrided samples were approximately the same, mainly Fe_2O_3, FeOOH. The corrosion products detected by XRD are mainly sulfides, whilst the corrosion products detected by XPS are mainly oxides. This is because the detection depth of the two techniques is different: the detection depth of XRD is usually in the micron range, but the XPS detection is in the nanoscale. Therefore, it can be considered that the corrosion product is layered with the oxide content enriched in the outer layer and the sulfide content in the inner layer.

The characteristic peaks of Cr in nitrided and untreated samples are mainly Cr_2O_3 and a small amount of $Cr(OH)_3$. Chromium accumulated in the corrosion product film to form a stable amorphous $Cr(OH)_3$, which makes the film more stable. At the same

time, the corrosion product film mainly containing Cr(OH)$_3$ has a certain cation selective permeability. It can effectively prevent the anion from penetrating the corrosion product film to the metal surface and reduce the corrosion rate of the material.[26] Since Cr(OH)$_3$ is amorphous,[27] it does not be detected by XRD.

For the S$_{2p}$ fit spectrum, 162.2 eV and 163.5 eV can be considered as the peak of FeS$_{1.15}$, which is consistent with the previous analysis. 168.6 eV can be considered as a characteristic peak of sulfate, such as FeSO$_4$, Fe$_2$(SO$_4$)$_3$, etc. The presence of sulfates was not expected to be formed in H$_2$S electrolyte due to the absence of oxygen in solution, which could be the consequence of sulfide oxidation during the air exposition between the end of aging in the H$_2$S solution and the XPS measurements. For the nitrided samples, 396.7 eV can be regarded as a characteristic peak of CrN in N$_{1s}$ fit spectrum. 399.6 eV can be regarded as a characteristic peak of NH$_4^+$, indicating that the active nitrogen of the nitrided layer reacts with H$^+$ in the H$_2$S solution, consumes H$^+$, lowers the pH and protects the metal. The experimental result is consistent with our previous finding.[28]

It can be found from Table 2 that after the H$_2$S corrosion, the S content (13.27 at%) and Fe content (12.51 at%) of the untreated sample are significantly larger than that of the nitrided sample (0.3 at% S and 1.93 at% Fe). On the one hand, it is shown that nitriding can prevent the formation of corrosion products on the surface of the sample, and on the other hand, it also indicates that the corrosion product is difficult to deposit on the surface of the sample. The literature indicates that under certain conditions, the corrosion product film has no protective effect on the substrate and may even lead to an increase in the corrosion rate.[29-31] Since the nitrided layer reduced the production of corrosion products, further corrosion of the sample can be prevented.

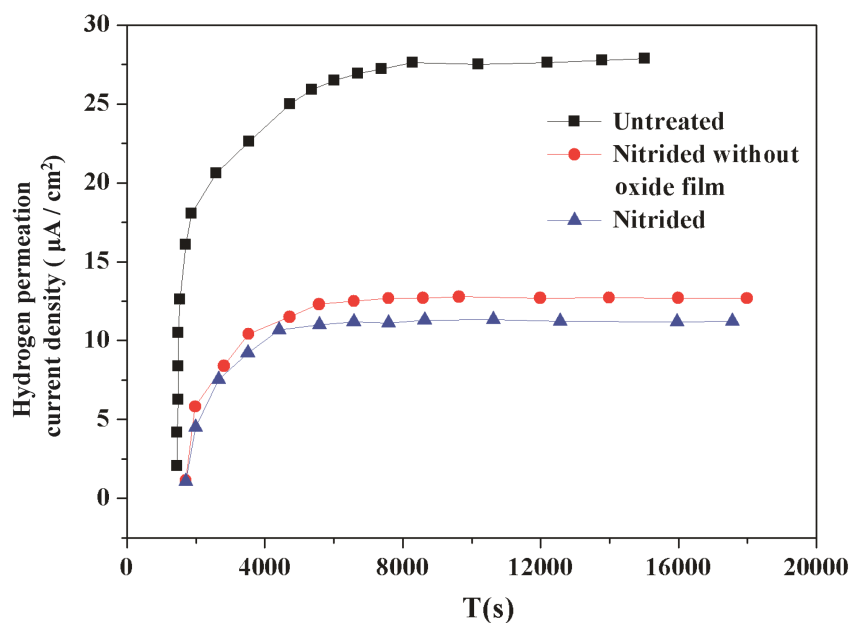## 3.6 Hydrogen permeation analysis

346

Fig.10 Hydrogen permeation current density curves of samples under different conditions.
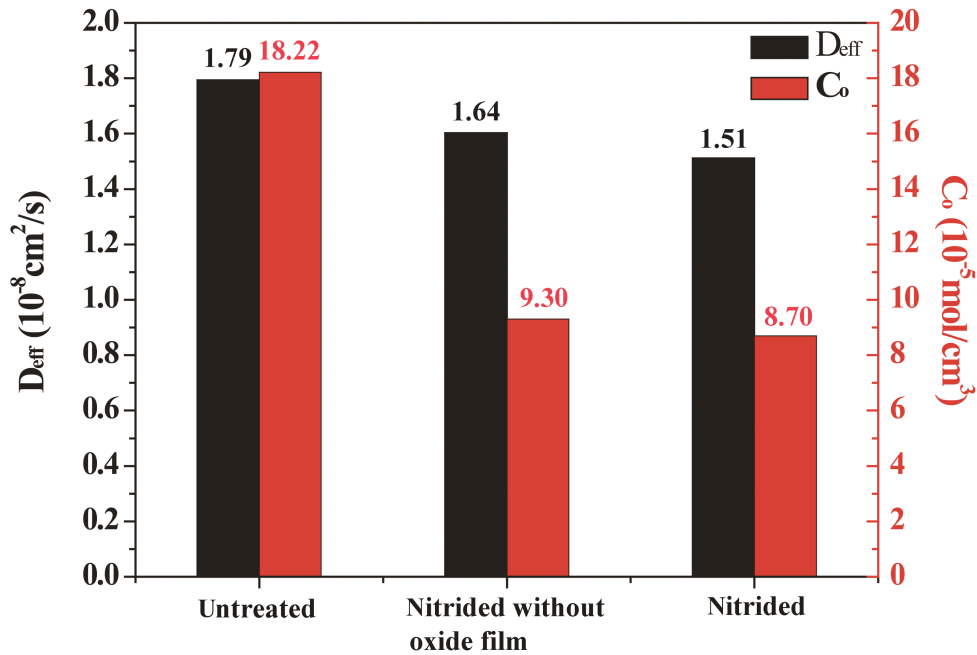
348

349

Fig .11 Diffusion coefficients and hydrogen atom concentrations curve of the sample under
351 different conditions.

352   Hydrogen permeation occurring on the surface of pipe steel is one of the main
353 risks of steel failure, and the intensity of which can be reflected in the hydrogen
354 permeation current. [32] Zhang et al. investigated the effect of the cathodic current
355 density (i) on the permeation of hydrogen through X80 pipeline steels using an
356 electrochemical permeation technique and they provided an equation to describe the
357 relationship between concentration of hydrogen (C_0) and cathodic current density (i),
358 this equation indicated that C_0 increased with i. [33] The hydrogen permeation current
359 density curves of different samples are shown in Figure 10. It can be seen that the
360 anodic steady-state current density of untreated samples is significantly greater than
361 that of as-nitrided samples and nitrided & oxide film removed samples. In addition，
362 the untreated sample took a longer period to reach the steady state anode current
363 density than the as-nitrided samples and the nitrided & oxide film removed samples.
364 Figure 11 shows the hydrogen diffusion coefficient D_{eff} and hydrogen concentration
365 C_0 for different materials states. The results show that the hydrogen concentration in
366 the untreated sample (18.22×10^{-5} mol/cm^2) is significantly higher than that of the
367 as-nitrided sample (9.30×10^{-5} mol/cm^2) and the nitrided & oxide film removed
368 samples (8.70×10^{-5} mol/cm^2). The reason for this may be that the nitrided layer could
369 trap a large amount of hydrogen, thus resulting in a substantial reduction of hydrogen
370 absorption by the substrate.[34] The hydrogen diffusion coefficient (1.79×10^{-8} cm^2/s) of
371 the untreated sample is larger than that of the as-nitrided sample (1.64×10^{-8} cm^2/s) and
372 nitride & oxide film removed sample (1.51×10^{-8} cm^2/s), indicating the nitrided layer
373 and oxide layer can reduce the diffusion coefficient of hydrogen.

4. **Discussion**

## 4.1 The effect of the nitrided layer on hydrogen permeation

When the sample is soaked in the H_2S containing solution for a long time, H_2S reacts with the surface of the steel to produce hydrogen, which then enters the steel matrix，building up pressure that leads to embrittlement.[35] Research has shown that supersaturated interstitials cause large lattice expansion while the non-nitrided bulk material constrains this expansion, causing the nitrided layer to have very high residual compressive stresses.[36] Therefore, the residual compressive stress helps to relieve the tensile stress caused by the H atoms, thus preventing hydrogen embrittlement. However, when the sample is in a stress corrosion environment and the applied tensile stress increases to a certain extent, the residual compressive stress of the S-phase layer may be cancelled out and hydrogen-induced cracking can occur.[28] From the results of electrochemical hydrogen permeation experiment (Fig.10 and Fig 11), it can be seen that both the nitrided layer and the oxide layer help reduce the diffusion coefficient of hydrogen and the amount of hydrogen atoms entering the material, thus shorting the time required for the anode current to reach equilibrium. The possible reason is that the nitriding layer can trap a large amount of hydrogen, resulting in a substantial reduction of hydrogen absorption by the substrate,[34] as shown in Figure 11.

Research has shown that electrochemical H-charging of pulsed plasma nitrided austenite resulted in a softening effect within the compound layer (S-phase).[37] The hydrogen in the lattice acts as a solution softening agent and the softening or hardening effect of the hydrogen is dependent on the nitrogen concentration and the dislocation density of the material. As can be seen from Figure 7, the nitrogen concentration exceeds 20 at%. When hydrogen ions enter the nitrided layer with a very high interstitial atom content, it softens and prevents hydrogen embrittlement.

4.2 The effect of the nitriding on H_2S corrosion

Figure 12 schematically shows the H_2S corrosion model for untreated and nitrided specimens. As shown in Figure 12(a), acidic H_2S solution hydrolyzes H^+, HS^-, S^{2-}，which reacts on the surface of the steel to produce Fe^{2+}. When acidic chemical corrosion occurs, the inherent protective film on the pipe surface is destroyed, causing the corrosive medium to enter the interior of the metal crystal and generating electrochemical corrosion. Electrochemical corrosion forms an etched primary cell. The anode process is a dissolution reaction of the metal, and the cathode undergoes a hydrogen depolarization reaction. Anodic sulphide corrosion products deposit on the metal surface, which is poorly protective and in fact promotes the corrosion of the stainless steel substrate. Monnot et al. highlighted the role of corrosion products on the failure mechanism of martensitic stainless steels in sour media.[38] Corrosion product formed under this condition has a high level of porosity and is prone to spalling due to cracks and defects throughout the amorphous structure. In fact, H_2S diffuses on the surface of the etching film and penetrates along the porous structure, and reacts at the metal/film interface. The metal sulphide is formed to release the hydrogen previously bound to the sulfur that can be absorbed by the alloy. Corrosion

product films therefore correspond to a rich hydrogen reservoir near the metal surface that can trigger and maintain hydrogen uptake. The data in Table 2 show that nitriding treatment can effectively reduce the generation of corrosion products, thereby alleviating hydrogen embrittlement and corrosion.
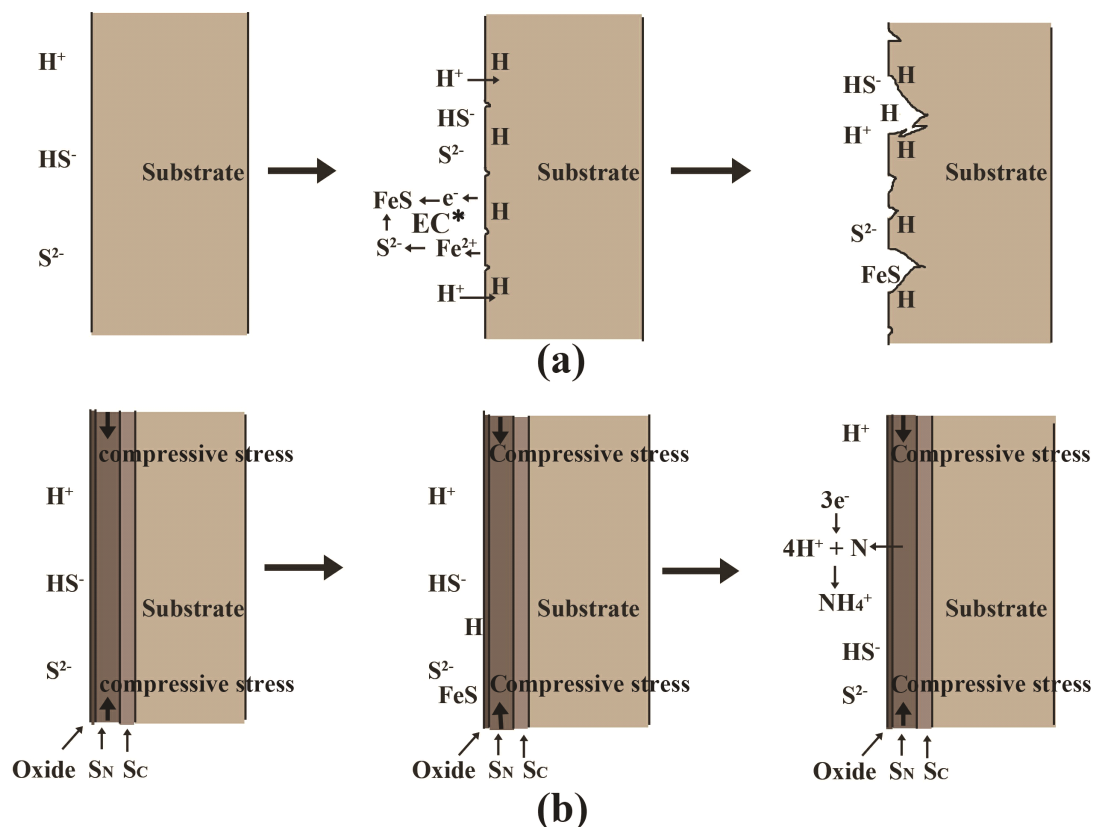
Note:* stands for electrochemical corrosion.

Fig.12 H_2S corrosion model of (a) untreated sample and (b) nitrided sample

The oxide layer can effectively prevent the corrosion of acidic H_2S as schematically shown in Figure 12(b). Granda—Gutiérrez et al. found that post-oxidation following nitriding treatment increased the time to SSC rupture of stainless steel by a factor of 10 because the dense oxide film on the surface after the treatment significantly improved the resistance to H_2S corrosion cracking of the stainless steel.[39] This is partially because the nitride layer reduced the generation of corrosion products (Table 2) and partially because it also prevented hydrogen atoms (Fig.11) from entering the substrate, thereby preventing electrochemical corrosion.

Nitrogen can effectively improve the local corrosion resistance of stainless steel,[40] and some hypotheses have been put forward to explain this behavior: (1) high concentration of nitrogen atoms on the surface of stainless steel stabilizes passive film and inhibits dissolution;[41-43] (2)formation of NO_3^- (nitrate) ions leads to increased pitting resistance;[44] (3) stabilization effect of nitrogen on austenite.[45] For the nitrided samples produced in this research, there are a large amount of active nitrogen

439 atoms in the surface of the sample after low temperature nitriding due to the high
440 level of chromium, nickel, molybdenum in the matrix material . The fitted spectra of
441 N1s from the nitriding samples after being soaked in H_2S solution are shown in Figure
442 9. H^+ reacts with the nitrogen atom via the reaction：$N + 4H^+ = NH_4^+$. This consumed
443 the H^+ in the solution prevented the pH of the metal surface from decreasing, and
444 thereby increased the corrosion resistance of the alloy, which is consistent with the
445 EPMA results in Figure7. At the same time, the active nitrogen atoms can accelerate
446 the formation of passivation film and affect the repassivation kinetics, so that the
447 passivation film can grow stably and increase the density of the passivation film.[46]

5. Conclusions

449   Low-temperature liquid nitrided samples have better corrosion resistance than
450 untreated samples in H_2S environment. The corrosion rate of the untreated sample is
451 about 3.6 times that of the nitriding sample; clear corrosion pits can be observed on
452 the surface of the untreated sample, while the treated sample surface remains almost
453 intact. Due to the presence of oxide layers, despite precipitation of CrN in the
454 nitriding layer, the corrosion resistance of the sample after the nitriding treatment in
455 the H_2S environment is still significantly improved by the treatment.

456   The corrosion products are mainly consisted of oxides, hydroxides, and sulfates.
457 The nitrided layer reduces the production of corrosion products; further corrosion of
458 the sample is thus prevented. Both oxide layer and nitrided layer can reduce the
459 diffusion coefficient of hydrogen and the amount of hydrogen atoms entering the
460 material, which is beneficial to improving the resistance to hydrogen embrittlement.
461 Nitriding layer is supersaturated with active nitrogen atoms, which combine with H^+
462 to avoid surface pH reduction, thus decelerating H_2S corrosion.

Acknowledgement

468

References

470 1.   K. Komai, *Int. J. Fatigue.,* 1998, vol. 20, pp. 145-154.
471 2.   M. L. Medvedeva and V. V. Gur'Yanov, *Prot. Met.,* 2002, vol. 38, pp. 284-288.
472 3.   D. W. Shoesmith, P. Taylor, M. G. Bailey and D. G. Owen, *Cheminform,* 1980, vol. 11, pp.
473 1007-1015.
474 4.   H. Yang, J. Chen, C. Cao, D. Cao and X. Jiang, *J .Chin. Soc. Corros . Rrot.,* 2001, vol. 21, pp.
475 321-327.
476 5.   H. Wang, P. Zhou, S. Huang, C. Yu, *Int. J. Electrochem. Sci.,* 2016, vol. 11, pp. 1293-1309.
477 6.   J. Fliethmann, H. Schlerkmann and W. Schwenk, *Corros. Sci.,*1992, vol. 24, p. 746.
478 7.   J. Ding, Z. Lei, M. Lu, J. Xue and Z. Wen, *J. Mater. Sci. Technol.,* 2013, vol. 48, pp. 3708-3715.
479 8.   S. K. Putatunda, *Mat. Sci. Eng. R.,* 1986, vol. 82, pp. L7-L11.

480   9.   W.T. Tsai and S.L. Chou, *Corros. Sci.,* 2000, vol. 42, pp. 1741-1762.

481   10.   L. F. Li, Z. Q. Huang and X. M. Liu, *Adv. Mater.,* 2012, vol. 485, pp. 393-396.

482   11.   A. Heuer and S. Collins, *Metall. Mater. Trans. A.,* 2009, vol. 40, pp. 1767-1767.

483   12.   G. M. Michal, F. Ernst, H. Kahn, Y. Cao, F. Oba, N. Agarwal and A. H. Heuer, *Acta. Mater.,* 2006,
484   vol. 54, pp. 1597-1606.

485   13.   X. Y. Li and H. Dong, *Met. Sci. J.,* 2003, vol. 19, pp. 1427-1434.

486   14.   S.J.B.Kurza, S.R.Mekaa, N.Schellb, W.Eckerc, J.Keckesd, E.J.Mittemeijerae, *Acta. Mater.,* 2015,
487   vol. 87,pp.100-110.

488   15.   L. Zhang, C. Ren, Q. Yu, J. Zhang, S. Sun, Q. Ren, Y. Lian, X. Chen and W. Gao, *Surf. Coat.*
489   *Technol.,* 2017, vol. 315, pp. 95-104.

490   16.   J. Wang, Y. Lin, J. Yan, D. Zeng, R. Huang and Z. Hu, *Isij Int.,*2012, vol. 52, pp. 1118-1123.

491   17.   M. A. V. Devanathan, Z. Stachurski, *Proc. Royal. Soc. Lond,* 1962, vol. 270(1340), pp. 90-102

492   18.   S. Shen, X. Li, P. Zhang, Y. Nan, G. Yang: *Mater. Sci. Eng. A* 2017, vol. 703, pp: 413-421

493   19.   H. Hu, K. Li, W. Wu, G.X.Chen, W.J.Chen: *J. Xi'an Jiaotong Univ.* 2016, vol. 50(07). 89-95.

494   20.   C. Zhou, S. Zheng, C. Chen and G. Lu, *Corros. Sci.,* 2013, vol. 67, pp. 184-192.

495   21.   R.A. Carneiro, R. C. Ratnapuli and V. D. F. C. Lins, *Mat. Sci. Eng. A.,* 2003, vol. 357, pp.
496   104-110.

497   22.   C. F. Dong, Z. Y. Liu, X. G. Li and Y. F. Cheng, *Int. J. Hydrogen. Energ.,* 2009, vol. 34, pp.
498   9879-9884.

499   23.   M. Tsujikawa, N. Yamauchi, N. Ueda, T. Sone and Y. Hirose, *Surf. Coat. Technol.,* 2005, vol. 193,
500   pp. 309-313.

501   24.   W. Shi, X. Y. Li and H. Dong, *Wear.,* 2001, vol. 250, pp. 544-552.

502   25.   M. Mantel and J. P. Wightman, *Surf. Interface. Anal.,* 1994, vol. 21, pp. 595-605.

503   26.   C. F. Chen, W. F. Chang, Z. H. Zhang, M. X. Lu and D. B. Sun, *Corrosion -Houston Tx-* 2005, vol.
504   61, pp. 594-601.

505   27.   J. Sun, C. Sun, X. Lin, X. Cheng and H. Liu, *Materials.,* 2016, vol. 9, p. 200.

506   28.   X. Zhang, J. Wang, H. Fan, J. Yan, L. Duan, T. Gu, G. Xian, L. Sun and D. Wang, *Metall. Mater.*
507   *Trans. A.,*2018, vol. 49, pp. 356-367.

508   29.   D. R Morris, L. P Sampaleanu and D. N Veysey, *J. Electrochem. Soc.,* 1980, vol. 127, pp.
509   1228-1235.

510   30.   F. H. Meyer, O. L. Riggs, R. L. Mcglasson and J. D. Sudbury, *Corrosion -Houston Tx-* 1958, vol.
511   14, pp. 109-115.

512   31.   J. S. Smith and J. D. A. Miller, *Brit. Corros. J.,* 2013, vol. 10, pp. 136-143.

513   32.   C. Zhou, X. Chen, Z. Wang, S. Zheng, X. Li, L. Zhang, Corros. Sci. 2014, vol. 89, pp: 30-37

514   33.   L. Zhang, W. Cao, K. Lu, Z. Wang, Y. Xing, Int. J. Hydrogen Ener, 2017, vol. 42(5), pp:
515   3389-3398.

516   34.   T. Zakroczymski, J. Flis, N. Lukomski and J. Mankowski, *Acta.Mater.,* 2001, vol. 49, pp.
517   1929-1938.

518   35.   Z. Y. Liu, C. F. Dong, X. G. Li, Q. Zhi and Y. F. Cheng, *J. Mater. Sci.,* 2009, vol. 44, pp.
519   4228-4234.

520   36.   A. H. Heuer, F. Ernst, H. Kahn, A. Avishai, G. M. Michal, D. J. Pitchure and R. E. Ricker, *Scripta*
521   *Mater.,* 2007, vol. 56, pp. 1067-1070.

522   37.   M. Asgari, A. Barnoush, R. Johnsen and R. Hoel, *Corros. Sci.,* 2012, vol. 62, pp. 51-60.

523   38.   M. Monnot, R.P. Nogueira, V. Roche, G. Berthomé, E. Chauveau, R. Estevez,M. Mantel, *Appl.*

524   *Surf. Sci.*, 2017, 394:132-141.

525   39.   E. E. Granda-Gutiérrez, J. C. Díaz-Guillén, J. A. Díaz-Guillén, M. A. González, F.

526   García-Vázquez and R. Muñóz, *J. Mater. Eng. Perform.,* 2014, vol. 23, pp. 4148-4153.

527   40.   P. G. Esteban, L. Bolzoni, E. M. Ruiznavas and E. Gordo, *Power. Metall.,* 2011, vol. volume 54,

528   pp. 242-252(11).

529   41.   Y. C. Lu, R. Bandy, C. R. Clayton and R. C. Newman, *Cheminform.,* 1983, vol. 14, pp.

530   1774-1776.

531   42.   H. Baba, T. Kodama and Y. Katada, *Corros. Sci.,* 2002, vol. 44, pp. 2393-2407.

532   43.   C.O. A. Olsson, *Corros. Sci.,* 1995, vol. 37, pp. 467-479.

533   44.   H. P. Leckie, *J.electrochem. soc.,* 1966, vol. 113, pp. 1262-1267.

534   45.   J. W. Simmons, *Mat. Sci. Eng. A.,* 1996, vol. 207, pp. 159-169.

535   46.   P. R. Levey and A. R. V.Bennekom, *Corrosion.,* 1995, vol. 51, pp. 911-921.